

Circular *ac* Hall Effect

J. Karch,¹ P. Olbrich,¹ M. Schmalzbauer,¹ C. Zoth,¹ C. Brinsteiner,¹ M. Fehrenbacher,¹
 U. Wurstbauer,¹ M. M. Glazov,² S. A. Tarasenko,² E. L. Ivchenko,² D. Weiss,¹
 J. Eroms,¹ R. Yakimova,³ S. Lara-Avila,⁴ S. Kubatkin,⁴ S. D. Ganichev¹
¹ Terahertz Center, University of Regensburg, 93040 Regensburg, Germany
² Ioffe Physical-Technical Institute, Russian Academy of Sciences, 194021 St. Petersburg, Russia
³ Linköping University, S-58183 Linköping, Sweden and
⁴ Chalmers University of Technology, S-41296 Göteborg, Sweden
 (Dated: November 9, 2018)

We report the observation of the circular *ac* Hall effect where the current is solely driven by the crossed *ac* \mathbf{E} - and \mathbf{B} -fields of circularly polarized radiation. Illuminating an unbiased monolayer sheet of graphene with circularly polarized terahertz radiation at room temperature generates - under oblique incidence - an electric current perpendicular to the plane of incidence, whose sign is reversed by switching the radiation helicity. Alike the classical *dc* Hall effect, the voltage is caused by crossed \mathbf{E} - and \mathbf{B} -fields which are however rotating with the light's frequency.

PACS numbers: 73.50.Pz, 72.80.Vp, 81.05.ue, 78.67.Wj

For more than a century, the Hall effect has enabled physicists to gain information on the electronic properties of matter. In Hall's original experiment [1], a clever combination of static magnetic and electric fields allowed to determine the sign and density of charge carriers, opening the door to a more thorough understanding of electronic transport in metals and semiconductors. The circular *ac* Hall effect (CacHE), in contrast, driven by the crossed *ac* \mathbf{E} - and \mathbf{B} -fields of circularly polarized light, delivers information on the underlying electron dynamics. The effect remained so far undiscovered as electromagnetic radiation incident upon low dimensional structures causes all sorts of photocurrents stemming from both contact and band-structure specifics. With respect to the latter the newly discovered graphene [2] is an ideal model system as symmetry prevents other helicity driven photocurrents like the circular photogalvanic [3] or spin-galvanic effect [4] to occur.

Two types of graphene were investigated: large area graphene prepared by high temperature Si sublimation of semi-insulating silicon carbide (SiC) substrates [5] and exfoliated graphene [2] deposited on oxidized silicon wafers. While both types of samples showed the effect, the micron sized exfoliated samples displayed an additional edge contribution (discussed in Ref. [6]) as the spot size of the terahertz (THz) laser of 1 mm^2 was larger than the graphene flakes. Hence, we focus on the large area SiC based samples having areas of 3×3 and $5 \times 5 \text{ mm}^2$. Both *n*- and *p*-type layers were probed. The experimental geometry is sketched in Fig. 1. The graphene samples were illuminated at oblique incidence, where the incidence angle θ_0 was varied between -40° and $+40^\circ$. The resulting photocurrent was measured at room temperature for wavelengths between $90 \mu\text{m}$ and $280 \mu\text{m}$ using either a continuous-wave (*cw*) CH_3OH laser or a high power pulsed NH_3 laser [10]. For these wavelengths the condition $\omega\tau < 1$ holds, with ω the angular frequency of

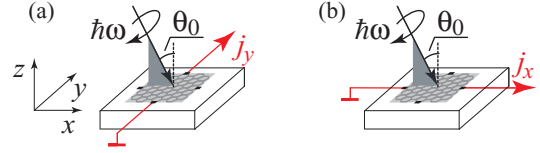


FIG. 1: Experimental configurations showing the plane of incidence of the radiation, the arrangement of contacts at the edges of graphene. Both (a) transverse and (b) longitudinal arrangements were used to measure the photocurrents.

the light and τ the momentum relaxation time of electrons (holes) in graphene. The resulting photocurrent is measured by the voltage drop across a load resistor between pairs of contacts made at the edges of the graphene square. To prove that the signal stems from graphene and not, e.g., from the substrate, we removed the graphene layer from one of the exfoliated samples and observed that the signal disappeared. The degree of circular polarization, $P_{\text{circ}} = \sin 2\varphi$, is adjusted by a quarter-wave plate, where φ is the angle between the initial polarization vector of the laser light and the *c*-axis of the plate.

The photocurrent for the transversal geometry, j_y , is shown in Fig. 2 as a function of φ . The principal observation made in all investigated samples is that for circularly polarized light, i.e. for $\varphi = 45^\circ$ and 135° , the sign of j_y depends on the light's helicity and the charge carriers' polarity. The overall dependence of j_y on φ is more complex and, at small θ_0 , well described by

$$j_y = A\theta_0 \sin 2\varphi + B\theta_0 \sin 4\varphi + \xi. \quad (1)$$

Here, ξ is a polarization independent offset, ascribed to sample or intensity inhomogeneities. It does not change with angle θ_0 and is subtracted from the data of Fig. 2. The fit parameters A and B describe the strength of the circular contribution $j_A \propto \sin 2\varphi$ and of the contribution $j_B \propto \sin 4\varphi$ caused by linear polarization. Both contri-

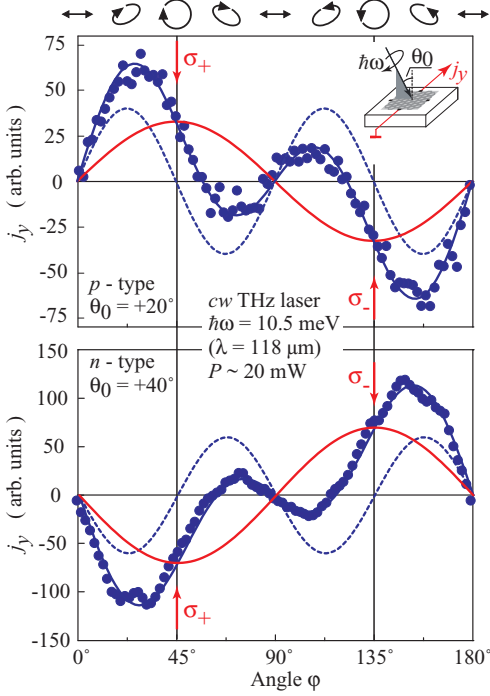


FIG. 2: Transverse photocurrent j_y as a function of the angle φ for p - and n -type graphene. The ellipses on top illustrate the polarization states for various φ . Full blue lines show fits to the calculated total current $j_A + j_B$ comprising the circular contribution j_A (CacHE, full red line) and the linear contribution j_B (dashed blue line).

Contributions are shown together with the resulting fit of the data in Fig. 2. Note that for purely circularly polarized light, the linear contribution j_B vanishes.

In the longitudinal geometry [Fig. 1(b)], only linearly polarized light gives rise to the φ -dependence of j_x :

$$j_x = B\theta_0(1 + \cos 4\varphi) + C\theta_0 + \xi'. \quad (2)$$

This is shown in the inset of Fig. 3 for both n - and p -type graphene. A sizable fraction of j_x stems from the polarization independent contribution $j_C = C\theta_0$, whose sign does not reverse with helicity. Both currents j_y and j_x , however, change their signs upon reversing the direction of incidence (Fig. 3).

The experimental data are well described by the theoretical model, outlined below. While the longitudinal currents can be explained along similar lines, we focus on the transverse helicity-driven current j_A . The basic physics behind the CacHE is illustrated in Fig. 4. Here, we consider the classical regime, where the photon energy is much smaller than the Fermi energy, $\hbar\omega \ll |E_F|$, fulfilled in the experiment as $|E_F|$ is ~ 100 meV while the photon energy $\hbar\omega$ is typically ~ 10 meV. For circularly polarized radiation, the electric field rotates around the wavevector \mathbf{q} , sketched in Fig. 4(a) for σ_+ circularly polarized light. This leads to an orbital motion of the holes (electrons) illustrated in Fig. 4. The CacHE comes

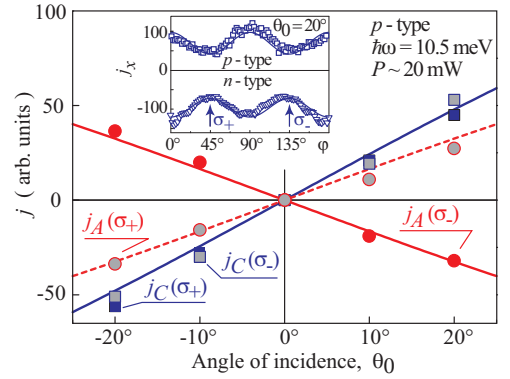


FIG. 3: Photocurrents j_A (red symbols) and j_C (blue symbols) induced by circularly polarized light σ_{\pm} ($\varphi = 45^\circ$ and 135°) as function of the incidence angle θ_0 . Open red circles and blue squares correspond to σ_+ , filled red circles and blue squares to σ_- . The inset shows the φ dependence of j_x measured both in p - and n -type graphene together with fits according to Eq. (2). The solid lines are fits based on Eqs. (4)-(5). The constant offsets ξ and ξ' have been subtracted.

into existence due to the combined action of the rotating electric and magnetic field vectors \mathbf{E} and \mathbf{B} , respectively. At an instant of time, e.g., at t_1 , the electron is accelerated by the in-plane component \mathbf{E}_{\parallel} of the ac electric field. At the same time, the electron with velocity \mathbf{v} is subjected to the out-of-plane magnetic field component \mathbf{B}_z . Note, that the velocity \mathbf{v} does not instantaneously follow the actual \mathbf{E}_{\parallel} -field direction due to retardation: There is a phase shift equal to $\arctan(\omega\tau)$ between the electric field and the electron velocity \mathbf{v} . Only for $\omega\tau \ll 1$ the directions of \mathbf{v} and \mathbf{E}_{\parallel} coincide. The effect of retardation, well known in the Drude-Lorentz theory of high frequency conductivity [11], results in an angle between the velocity \mathbf{v} and the electric field direction \mathbf{E}_{\parallel} , which depends on the value of $\omega\tau$. The resulting Lorentz force $\mathbf{F}_L = e(\mathbf{v} \times \mathbf{B}_z)$, where e is the positive (holes) or negative (electrons) carrier charge, generates a Hall current \mathbf{j} , also shown in Fig. 4. Half a period later at $t_2 = t_1 + T/2$, both \mathbf{v} and \mathbf{B}_z get reversed so that the direction of \mathbf{F}_L and, consequently, the current \mathbf{j} stay the same. The oscillating magnitude and direction of \mathbf{B}_z along the closed trajectory leads to a periodical modulation of the Lorentz force with non-zero average causing a non-zero time-averaged Hall current with fixed direction.

If, as shown in Fig. 4(c), the light helicity is reversed, the electric field rotates in the opposite direction and, thus, the carrier reverses its direction. Hence, the y -component of \mathbf{F}_L at t_1 and t_2 is inverted. Consequently the polarity of the transverse, time-averaged Hall current changes. This is the circular ac Hall effect. On the other hand, we obtain the longitudinal current j_x , which does not change direction when the helicity flips. This current is also observed in our experiment, displayed in Fig. 3. Obviously, flipping the angle of incidence, $\theta_0 \rightarrow -\theta_0$,

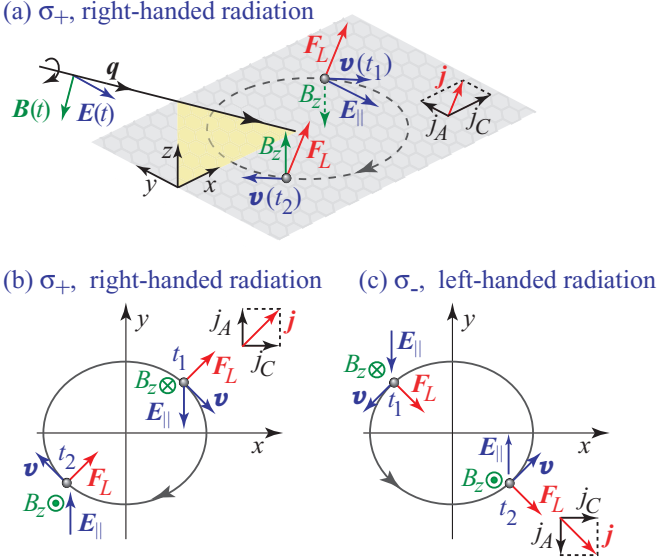


FIG. 4: Schematic illustration of the circular *ac* Hall effect. For simplicity we assume positive carriers, i.e. holes. (a) \mathbf{E} - and \mathbf{B} -field vectors of σ_+ polarized light with wave vector \mathbf{q} under oblique incidence in the (xz) plane. The solid orbit represents the hole's elliptical trajectory caused by the *ac* \mathbf{E} -field. The relevant vectors are shown for two instants in time, t_1 and t_2 , shifted by half a period. \mathbf{v}_1 and \mathbf{v}_2 are the hole velocities at t_1 and t_2 , respectively, taking retardation into account. The direction of the Lorentz force \mathbf{F}_L due to the *ac* \mathbf{B} -field determines the direction of the Hall current \mathbf{j} . (b) Top view of (a). (c) Same as (b) but for σ_- light.

results in a change of the relative sign of \mathbf{E}_{\parallel} and \mathbf{B}_z so that both j_x and j_y flip directions.

While the explanation of the CaCHE has been given in a pictorial way above, we resort now to a microscopic description based on the Boltzmann kinetic equation for the electron distribution function $f(\mathbf{p}, \mathbf{r}, t)$, with the free-carrier momentum \mathbf{p} , in-plane coordinate \mathbf{r} , and time t :

$$\frac{\partial f}{\partial t} + \mathbf{v} \frac{\partial f}{\partial \mathbf{r}} + e(\mathbf{E} + \mathbf{v} \times \mathbf{B}) \frac{\partial f}{\partial \mathbf{p}} = Q\{f\}. \quad (3)$$

Here, $Q\{f\}$ is the collision integral described in terms of momentum relaxation times τ_n ($n = 1, 2, \dots$) for corresponding angular harmonics of the distribution function. The electric current density is given by the standard equation $\mathbf{j} = 4e \sum_{\mathbf{p}} \mathbf{v} f(\mathbf{p})$, where a factor of 4 accounts for spin and valley degeneracies. In order to solve the kinetic equation (3), we expand the solution in powers of electric and magnetic fields, keeping linear and quadratic terms only. In the calculation of $f(\mathbf{p})$ and \mathbf{j} , we used the energy dispersion $\varepsilon_p = \pm v p$ of free carriers in graphene and the relation $\mathbf{v} \equiv \mathbf{v}_p = v \mathbf{p}/|p|$ between the velocity and the quasi-momentum ($v \approx c/300$, with c being the speed of light). Contributions to the photocurrent appear not only from a combined action of the electric and magnetic fields of the light wave, illustrated in Fig. 4, but also due to the spatial gradient of the electric field [12].

As final result we obtain for the helicity driven current

$$j_A = A \theta_0 \sin 2\varphi = q \theta_0 \chi P_{\text{circ}} \left(1 + \frac{\tau_2}{\tau_1} \right) \frac{1-r}{1+\omega^2 \tau_2^2}, \quad (4)$$

flowing in y -direction, and the φ -independent current

$$j_C = C \theta_0 = \frac{q \theta_0 \chi}{\omega \tau_1} \left[2(1+r) + (1-r) \frac{1-\omega^2 \tau_1 \tau_2}{1+\omega^2 \tau_2^2} \right], \quad (5)$$

flowing along x (for light propagating in the (xz) plane). Here $q = \omega/c$, $q \sin \theta_0 \approx q \theta_0$, $r = d \ln \tau_1 / d \ln \varepsilon$ and $\chi = e^3 \tau_1 (v \tau_1 E)^2 / [2 \pi \hbar^2 (1 + \omega^2 \tau_1^2)]$.

The results of the calculation are shown in Figs. 3 and 5. The used fitting parameters only depend on details of the underlying scattering mechanism discussed below. Equation (3) provides in addition to j_A and j_C also currents generated by linearly polarized light, $j_{B,x} \propto q \theta_0 (1 + \cos 4\varphi)$ and $j_{B,y} \propto q \theta_0 \sin 4\varphi$. These currents with different angular dependencies are superimposed on the circular *ac* Hall effect (and also on j_C discussed above), when φ is varied, and cause a more complex polarization dependence of the photocurrent (see blue lines in Figs. 2 and in the inset of Fig. 3). However, for perfect circularly polarized light ($\varphi = 45^\circ$ or 135°), the degree of linear polarization is zero and the corresponding currents vanish leaving the undisturbed CaCHE contribution, as shown in Figs. 2 and 3.

As seen in experiment the polarity of the photocurrents is opposite for n - and p -type graphene samples. This is expected from theory since (i) the *ac* Hall current j_y as well as the longitudinal current j_x are proportional to e^3 and (ii) the conduction- and valence-band, in the massless Dirac model, are symmetric with respect to the Dirac point. In contrast, in typical semiconductors conduction- and valence-band states have different symmetry properties and the relation between values and polarities of the *ac* Hall photocurrents is more involved.

Equations (4) and (5) suggest a non-monotonous frequency dependence of the photocurrents. In Fig. 5 the calculated frequency dependence of both $A = j_A/\theta_0$ and $C = j_C/\theta_0$ are compared quantitatively to experimental data. For the momentum scattering time we used the relation $\tau_1 = 2\tau_2 \propto \varepsilon_p^{-1}$, valid for short range scattering [13] and relevant for our low mobility samples. The carrier density $n = 3.8 \times 10^{12} \text{ cm}^{-2}$ and momentum scattering time $\tau_1 \approx 2 \times 10^{-14} \text{ s}$ were obtained from transport measurements. Apart from the above assumption of short range scattering, no fit parameter was used. Figure 5 shows that the theory describes the frequency dependence and the absolute value of the photocurrent very well. Both j_A and j_C contribute to the photocurrent for circularly polarized light. It is remarkable that the helicity driven current j_A and the polarization independent photocurrent j_C show completely different frequency dependencies. While j_C does not change much for $\omega\tau \ll 1$, j_A increases with growing $\omega\tau$ at low frequencies. For large $\omega\tau$ well above unity both photocurrents

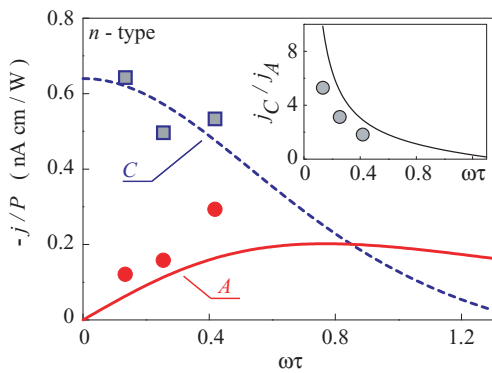


FIG. 5: Frequency dependence of $A = j_A/\theta_0$ (red dots) and $C = j_C/\theta_0$ (blue squares) as function of $\omega\tau$ for circularly polarized light. Data are shown for wavelengths between $90 \mu\text{m}$ and $280 \mu\text{m}$ with the power ranging from 10 kW to 30 kW. The photocurrent j_C is obtained from the current in x -direction, which for σ_+ , σ_- -light reads $j_x = C\theta_0$. The calculated frequency dependence of j_A (Eq. (4), red solid line) and j_C (Eq. (5), dashed line) describe the experiment quantitatively well. The inset shows j_A/j_C both for experiment and theory. This plot, independent of the absolute values, shows that the helicity driven current j_A vanishes for $\omega\tau \ll 1$.

decrease with increasing ω . This property agrees with the model addressed above The CaCHE, i.e. j_A , disappears for $\omega \rightarrow 0$, since no circular polarization exists for static fields and the required retardation vanishes. With increasing ω the retardation becomes important and the current increases $\propto \omega\tau$. For $\omega\tau \simeq 1$ the current gets maximal and decreases rapidly at higher ω , $j_y \propto 1/\omega^4$. In contrast, the longitudinal current j_C does not depend on the frequency at $\omega\tau \ll 1$ and displays its maximum at $\omega \rightarrow 0$. The effect of retardation is just opposite to that on j_A : Increasing ω reduces the y -component of the velocity (Fig. 4) and hence the x -component of the Lorentz force. As a consequence, j_C drops with increasing ω , see Fig. 5. The ratio of j_C and j_A is plotted in the inset of Fig. 5 showing that the role of the circular effect substantially increases with $\omega\tau$. The excellent agreement of theory and experiment shows that the model covers the essential physics of the circular ac Hall effect.

The photocurrents j_C and j_A are both proportional to the wavevector q and may, therefore, also be classified as photon drag effect. In fact, the polarization independent longitudinal current j_C is the well-known linear photon drag effect, which was first treated by Barlow [14] in 1954, observed in bulk cubic semiconductors [15, 16] and recently discussed for graphene [6, 17]. The circular ac Hall effect, described here, can be considered as the classical limit ($\omega\tau < 1$) of the circular photon drag effect. The latter effect which takes over at higher frequencies, i.e. for $\omega\tau > 1$, was discussed phenomenologically [18, 19] and observed in GaAs quantum wells in the mid-infrared range [20]. In this pure quantum mechan-

ical limit the picture above is inapplicable and involves asymmetric optical transitions and relaxation in a spin polarized non-equilibrium electron gas. The drag effect in metallic photonic crystals, generating a transverse current due to microscopic voids, was reported recently [21].

The appearance of a helicity driven Hall current is a specific feature of two-dimensional, even centrosymmetric, structures like graphene. CaCHE is a general phenomenon and should exist in any low-dimensional system. It is however more readily observable in a monoatomic layer like graphene, as in multilayered low-dimensional systems, e.g. quantum wells, the CaCHE is masked by the circular photogalvanic effect [3]. In monoatomic layers studied here, however, all photogalvanic effects vanish, since they require an electronic response to the out-of-plane component of the electric field. Using graphene therefore allowed us to identify the circular ac Hall effect unambiguously, thus providing a novel access to charge carrier dynamics and scattering.

We thank J. Fabian, V.V. Bel'kov, J. Kamann, and V. Lechner for fruitful discussions and support. Support from DFG (SPP 1459 and GRK 1570), Linkage Grant of IB of BMBF at DLR, RFBR, Russian Ministry of Education and Sciences, President grant for young scientists and "Dynasty" Foundation ICFPM is acknowledged.

-
- [1] E. H. Hall, *Amer. J. Math.* **2**, 287 (1879).
 - [2] K. S. Novoselov *et al.*, *Science* **306**, 666 (2004).
 - [3] E. L. Ivchenko and S. D. Ganichev, in *Spin Physics in Semiconductors*, ed. M. I. Dyakonov (Springer, 2008).
 - [4] S. D. Ganichev *et al.*, *Nature* **417**, 153 (2002).
 - [5] A. Tzalenchuk *et al.*, *Nature Nanotech.* **5**, 186 (2010).
 - [6] J. Karch *et al.*, arXiv:1002.1047v1 (2010).
 - [7] K. V. Emtsev *et al.*, *Nature Mat.* **8**, 203 (2009).
 - [8] C. Virojanadara *et al.*, *Phys. Rev. B* **78**, 245403 (2008).
 - [9] A. Bostwick *et al.*, *Nature Phys.* **3**, 36 (2007).
 - [10] S. D. Ganichev and W. Prettl, *Intense Terahertz Excitation of Semiconductors* (Oxford Univ. Press, 2006).
 - [11] N. W. Ashcroft and N. D. Mermin, *Solid State Physics* (Thomson Learning, 1976).
 - [12] V. I. Perel' and Ya. M. Pinskii, *Sov. Phys. Solid State* **15**, 688 (1973).
 - [13] S. Das Sarma *et al.*, arXiv:1003.4731v1 (2010).
 - [14] H. M. Barlow, *Nature* **173**, 41 (1954).
 - [15] A. M. Danishevskii *et al.*, *JETP* **31**, 292 (1970).
 - [16] A. F. Gibson *et al.*, *Appl. Phys. Lett.* **17**, 75 (1970).
 - [17] M. V. Entin *et al.*, *Phys. Rev. B* **81**, 165441 (2010).
 - [18] E. L. Ivchenko and G. E. Pikus, in *Problems of Modern Physics*, eds. V. M. Tuchkevich and V. Ya. Frenkel (Nauka, 1980) [*Semiconductor Physics*, eds. V. M. Tuchkevich and V. Ya. Frenkel (Cons. Bureau, 1986)].
 - [19] V. I. Belinicher, *Sov. Phys. Solid State* **23**, 2012 (1981).
 - [20] V. A. Shalygin *et al.*, *JETP Lett.* **84**, 570 (2006).
 - [21] T. Hatano *et al.*, *Phys. Rev. Lett.* **103**, 103906 (2009).